Hf and Pb isotope data for mafic lava flows from the Three Sisters and Newberry region of the central Oregon Cascades

by

Kyeong Pil Kong

Advisor: Dr. Euan C. Mitchell

Senior Honors Thesis
For the fulfillment of the requirements
For the degree of

Bachelor of Science
Geology

Washington and Lee University
Lexington, Virginia

April 2015

Acknowledgements

This project was supported by multiple funding sources with ties to Washington and Lee University:

Department of Geology at Washington and Lee
Robert E. Lee Summer Scholar's Program
Lenfest Research Grant
Johnson Opportunity Grant
R. Preston Hawkins IV Geology Endowment

I would like to first and foremost thank Dr. Euan C. Mitchell for his guidance throughout the entirety of the project. This project would not have been possible without his training, support, guidance, and expertise in this field of study.

I would also like to thank Dr. Yemane Asmerom, Victor Polyak, and the Department of Earth and Planetary Sciences at the University of New Mexico. All of the instrumental analyses were conducted in Dr. Yemane Asmerom's Radiogenic Isotope Laboratory at UNM. Victor Polyak provided crucial assistance in many aspects of laboratory work at the Radiogenic Isotope Laboratory and usage of the MC-ICP-MS.

This project would not have been successful without the support of my friends, peers, professors, and family. I owe it to all of them for my academic endeavors and achievements throughout my four years at Washington and Lee University as I look forward to enriching my knowledge and exposure of earth sciences in the near future.

Abstract

The Cascade arc is an end member convergent margin in which the young and slowly subducting slab is hotter than in most subduction zones. Consequently, the timing and location of slab contribution, namely dehydration, is impacted and ultimately affects the generation of magma in the overlying mantle. In order to constrain the extent of involvement of slab-derived components such as the subducting altered oceanic crust (AOC), sediments, and hydrated mantle lithosphere, radiogenic isotope ratios of mafic lava flow samples of interest were measured and modeled as mixtures of these end-members.

Prior work has measured major and trace elements, U-series (U-Th-Ra-Pa), and Sr-Nd isotopes from mafic lava flow samples from the Three Sisters volcano region (main-arc) and the Newberry Volcanic Field (back-arc) at the University of New Mexico's Earth and Planetary Sciences. These analyses indicate limited involvement of subducted sediments during magma generation.

Pb and Hf isotope data were collected on the same mafic lava flow samples from the previous work mentioned above. Ranges in Pb and Hf ratios, the first Hf data from the Oregon Cascades, are consistent with existing Cascade arc data: $^{206}Pb/^{204}Pb = 18.821–19.022$, $^{207}Pb/^{204}Pb = 15.576–15.617$, $^{208}Pb/^{204}Pb = 38.391–38.424$, and $^{176}Hf/^{177}Hf = 0.283032–0.283094$ ($\varepsilon_{Hf} = 9.19–11.38$). The most primitive lavas define a narrower range of $^{176}Hf/^{177}Hf$ values, with $\varepsilon_{Hf} > 10.28$. The most primitive lavas also define narrower ranges in Pb isotope ratios, intermediate between the Three Sisters and Newberry basaltic andesites.

Slab component models were created for Sr, Nd, Pb, and Hf isotopes; using elemental and isotopic values for Juan de Fuca MORB to represent a homogeneous mantle end member and data from ODP and DSDP drill sites on the Juan de Fuca plate to represent the sediment end member in the modeling systems. A variety of modeling scenarios suggest that the most likely slab contribution process is dehydration at relatively warm temperatures followed by a melting episode of the subducting sediments at higher temperatures. The sediment contribution from the subducting slab is estimated to range from 0.2 – 1.0%. Analysis of accessory phases in the melt residue qualitatively reaffirms the observations made from the slab component mixing models, indicating that volcanism in the central Oregon Cascade arc is driven by dehydration of the slab and melting of the subducting sediments at high temperatures.

Table of Contents

Introduction

The Cascade arc is an end member arc system that has been heavily studied to gain a better understanding of magma production in arc settings globally and regionally. Mantle melting in arcs occurs in response to dehydration of hydrous components within the subducting slab, which is composed of the subducting sediments, altered oceanic crust (AOC), and hydrated mantle lithosphere (Grove et al., 2002; Tatsumi, 1995). Dehydration fluids lower the peridotite solidus, thus producing melts in the subarc mantle wedge. Consequently, volcanism in the Cascades is assumed to be driven by dehydration of the obliquely subducting Juan de Fuca plate (Hildreth, 2007). The Juan de Fuca Ridge spreads at a rate of 25-35 mm/year, and is less than 11 Ma at the trench (Govers and Meijer, 2001). This relatively young plate remains warms as it subducts beneath the North American plate, which causes the thermal conditions of the arc to be hotter than other those of other arcs (Xue and Allen, 2007). Subducting slabs in most arcs begin to lose considerable amounts of water at depths greater than 80 km, while the subducting slab in the Cascades reaches hot enough temperatures for dehydration at approximately 50 - 75 km (Spandler and Pirard, 2013). Thermal modeling of the Juan de Fuca plate suggests that the slab surface temperature ranges from 850 - 950°C at sub-arc depths, which is relatively hot compared to other global arcs (Ruscitto et al., 2010; Syracuse et al., 2010). From the shallow dehydration, the warm slab becomes anhydrous at depths beyond the volcanic arc and reduces the fluxing of the deeper mantle wedge (Wada et al., 2008).

Radiogenic isotopes are sensitive indicators of contributions from the subducted oceanic crust and sediment that can help determine the thermal condition of the slab signature incorporated into the magma (Mullen and Weis, 2013). However, the mechanisms of slab contribution to the mantle wedge are still unknown to this day, and elemental data are complicated by subsequent mantle melting processes.

This project contributes Pb and Hf isotopic data for mafic lava flows from the Three Sisters and Newberry region of the central Oregon Cascades. Previous work done in this area provides elemental and some isotope data (U-Th-Ra-Pa, Sr-Nd) from the same samples analyzed in this project (Mitchell, 2013). Data from the previous work, along with the new Pb and Hf isotope data, were used in the modeling in an attempt to determine how and to what extent the dehydration of the subducting slab and sediments contribute to the composition of the lava flows from the study area.

Of primary concern is assessing heterogeneity of the mantle wedge and obtaining representative data for the sediments subducting beneath the study area for modeling purposes. One school of thought asserts that the diversity of mafic magma compositions in the Cascades can be attributed to mantle source heterogeneity, arguing that enriched intra-plate magmas cannot be generated from a depleted mantle source (DMM) (Churikova, 2001; Conrey et al., 1997; Hochstaedter et al., 2001; Leeman et al., 2005; Rowe et al., 2009). Conversely, others argue that mantle heterogeneity may play a minimal role in the genesis of magmas, ascribing differences in magma composition in the Cascades to variations in the degree of flux melting induced by subducted fluids (Green and Sinha, 2005; Reiners et al., 2000; Stolper and Newman, 1994). Since the dehydration of fluids is the main focus of this study and the data doesn't require multiple mantle sources, a homogeneous mantle source will be assumed. In addition, sediment data from multiple drilling sites in the Juan de Fuca plate will be used in order to minimize errors in the modeling.

Geologic Setting and Background

The Cascade arc is composed of over 2300 Quaternary volcanoes and extends approximately 1250 km from Mt. Lassen in California, United States, to Mt. Meager in British Columbia, Canada (Hildreth, 2007). There are a plethora of mafic vents in the Cascades, especially in the Three Sisters and Newberry area (Figure 1) (Conrey et al., 2002). Lavas from mafic vents volumetrically represent a large fraction of the Pliocene and Quaternary volcanic eruptions of the Oregon Cascades, and represent all of the compositional diversity of mafic magmas erupted within the main and back arc (Conrey et al., 2002; McBirney and White, 1982).

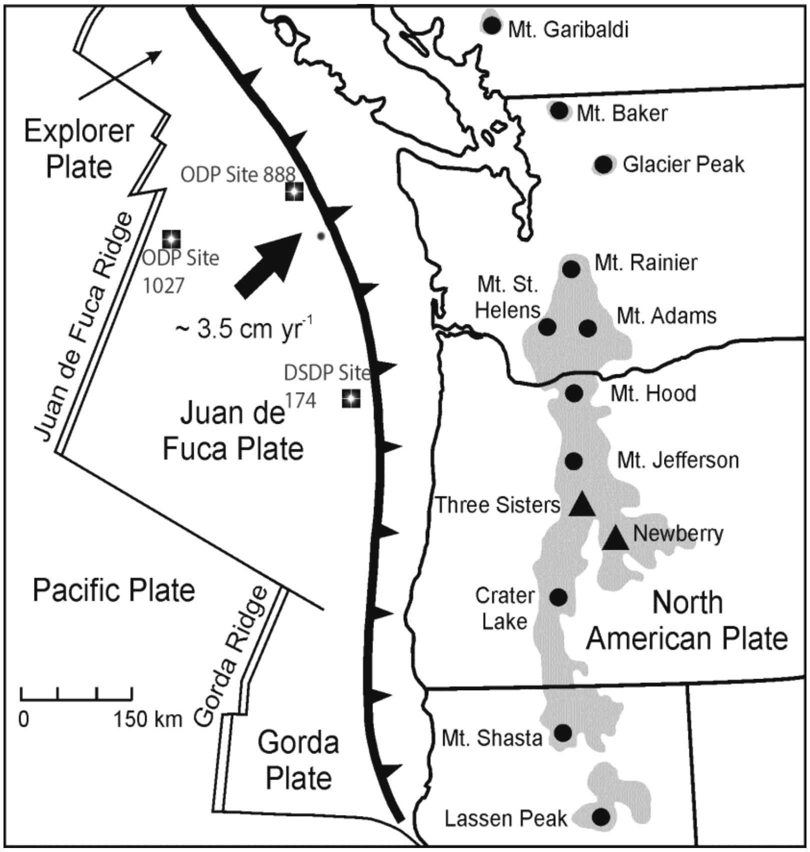

Figure 1: Tectonic setting of the Cascadia arc. The Juan de Fuca plate (spreading center located on the double and single lines; trench on the bold black line, teeth on the overriding plate) subducts to the northeast beneath the North American plate at ~ 3.5 cm/year. The study area, the Three Sisters volcanoes and Newberry Volcanic Field (triangles), is part of the Cascade arc (prominent volcanoes marked by circles). Sediment drilling sites (white stars) marked on the JdF plate were used as sediment end member proxies in all of the slab contribution mixing models (Carpentier 2014, Plank 2014). Map adopted from Mitchell (2011).

Basalts erupted in arc settings are predominantly subalkaline, having major element concentrations broadly similar to Mid Ocean Ridge Basalts (MORB) (Mullen and Weis, 2013). In addition, arc basalts have a characteristic 'slab' signature that is best expressed in trace element concentrations, such as a depletion in high field strength elements (HFSE) and enrichment in large ion lithophile elements (LILE) (Pearce and Stern, 2006).

In addition to the broad compositional properties of the lavas generated in the arc, geochemical and petrological analysis throughout the Cascades indicates that the mafic magmas are compositionally diverse (Mitchell and Asmerom, 2011). The Cascades' compositional diversity, based on trace element composition, includes low-K tholeiitic basalt, ocean island-like basalt, calc-alkaline basalt, shoshonitic basalt, and high-Mg basaltic andesite, and may be driven by the unique thermal conditions of the arc (Conrey et al., 1997).

A significant amount of isotopic data has been collected from many volcanic regions of the Cascades (e.g. Mt. Lassen, Mt. Adams, Mt. Garibaldi, Mazama) (Bacon et al., 1994; Borg et al., 2000; Jicha et al., 2009; Schmidt et al., 2008). Geochemical analyses of Juan de Fuca, Explorer, and Gorda MORB, in addition to sediments from the Juan de Fuca plate through drilling projects (ODP 888,1027; DSDP 174), have also been conducted (Cousens et al., 1995; 1985; Davis et al., 2008; Carpentier et al., 2014; Prytulak et al., 2006; Plank et al., 2014). The Three Sisters and Newberry regions, however, did not have much geochemical data until developments in the past few years (Mitchell, 2013).

The sampling area mainly comprises Mt. Jefferson, Mt. Washington, and Three Sisters Wilderness areas, along with mafic flows on the western flanks of Newberry volcano (Figure 2) (Mitchell, 2013). The Three Sisters group is part of the main arc, and Newberry shield volcano, located roughly 100 kilometers southeast of the Three Sisters, is part of the back arc (Hildreth, 2007). Crustal thickness in this area ranges from approximately 35 to 45 km, with Newberry representing the thinner section of the crust in this area (Eagar et al., 2011). Almost every mafic Holocene flow in the Three Sisters area and large flows from Newberry were collected for this study. Sampling a wide variety of lava flows from multiple vents in the study area increases the likelihood of encompassing a significant amount of the compositional variety represented in this region of the arc, where magmatism extends over 100 km from the fore-arc into the back-arc (Guffanti and Weaver, 1988).

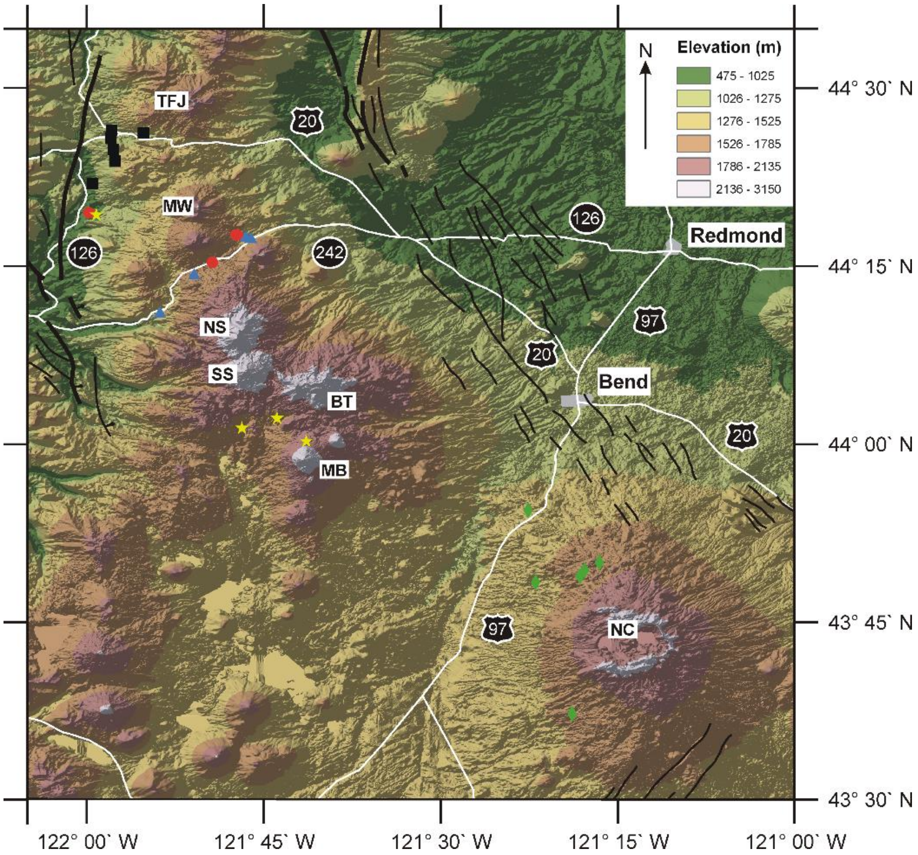

Figure 2. Shaded relief map of the study area within the central Oregon Cascades. Prominent volcanoes are labeled: TFJ = Three Fingered Jack, MW = Mt. Washington, NS = North Sister, SS = South Sister, BT = Broken Top, MB = Mt. Bachelor, and NC = Newberry caldera. Sample localities, grouped by vent location, are indicated with small symbols. Black squares = Sand Mountain group; red circles = Belknap group; blue triangles = Yapoah group; green diamonds = Newberry group; yellow stars = pre-Mazama group. Map adopted from Mitchell (2011).

Prior geochemical analyses of the same samples analyzed in this project indicate that the generation of these magmas results from decompression melting of the garnet-bearing enriched mantle wedge through mantle upwelling, along with limited fluid involvement from the dehydration of subducting sediments (Mitchell, 2013). Volatile fluxing, a common process in magma genesis in arcs, is inferred to be not as prevalent in generating these lavas due to the early and extensive dehydration of the subducting slab.

Uranium-series (U-series) studies on the same samples suggest that there are two processes of differentiation of primitive magmas that are influenced by the thermal and structural condition of the arc crust (Mitchell, 2013). Analysis of the Three Sisters data indicates that differentiation in the main arc is dominated by mixing between the upwelling primitive magmas and water-rich magmas in the lower crust. However, samples from Newberry, in the rear arc, indicate that primitive magmas here differentiate mainly through assimilation of the felsic upper crust (Mitchell, 2013). In this study, emphasis will be placed on modeling with the most primitive samples in order to study the process of dehydration as opposed to differentiation of the magma.

Samples and Methods

Twenty-four samples were collected in the Three Sisters volcanoes and Newberry volcano regions of the Cascade Range by Dr. Euan Mitchell (Mitchell and Asmerom, 2011). Of the twenty-four, eighteen were from the Three Sisters region (representing sixteen separate flows), categorized into four groups based on vent location (Belknap, pre-Mazama, Sand Mountain, and Yapoah). The remaining six samples were from six separate flows located on the flanks of Newberry volcano. Prior work has identified these samples as mafic lavas that are distinct in their trace element and isotopic composition (Figure 3) (Bas et al., 1986; Mitchell, 2013). In addition to the trace element and isotopic work, U-series data have also been obtained that include ^{238}U, ^{235}U, ^{230}Th, ^{226}Ra, and ^{231}Pa measurements.

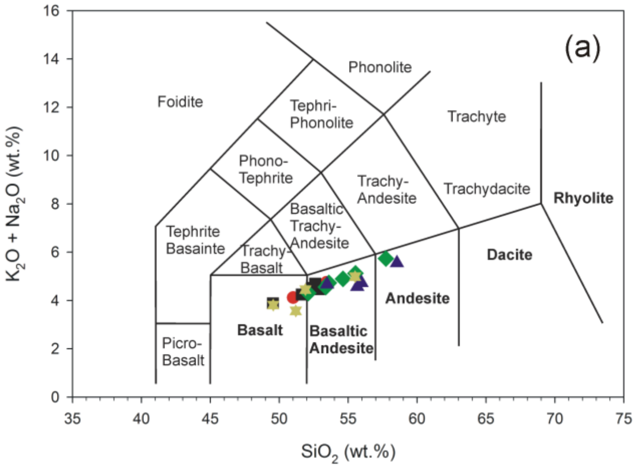

Figure 3: SiO_2 vs. ($K_2O + Na_2O$) plot with IUGS classification scheme (Le Bas et al. 1986). Symbols as Figure 2. Graph adopted from Mitchell (2013).

Primitive lavas have been previously identified in the broader sample suite and play a significant role in the isotopic analysis of the slab contribution due to the minimal influence of the overlying crust. Four primitive samples, 08-LL-01, Nash Crater; 08-WBB-01, Belknap; and 08-CYC-01/08-WIC-01, pre-Mazama have been identified following standard criteria (SiO_2 < 55 wt.%, MgO > 6 wt.%, Mg# (molar MgO/(MgO + FeO)*100) > 55, Ni > 100 ppm, and Cr > 200 ppm) (Leeman et al., 2005). The most primitive Newberry sample (08-SPBF-01), although not meeting all of these criteria, is included in this group in the analysis that follows to allow a comparison between the main and rear arc.

Hf and Pb isotope analyses were conducted in the Radiogenic Isotope Lab at the University of New Mexico. A single powder batch was used to separate Pb and Hf following a procedure modified from Weis et al. (2006) and Connelly et al. (2006), respectively. Approximately 0.130 g of powdered sample was weighed out and placed into a Teflon bomb with a mixture of 0.75 mL 15N HNO_3 and 5mL 28N HF. This mixture was placed in an oven to dissolve at 125°C for approximately 48 hours. The solution was then transferred to a Teflon beaker with 15N HNO_3, and then placed on a hot plate until complete dryness. After drying, approximately 2 mL of 15N HNO_3 was added to dissolve the solid, and fluxed for several hours to ensure that the sample had dissolved. Then, 0.8 mL of 3.5N HNO_3 + 0.45N H_3BO_3 along with 4mL of 9.6N HCl was added to the dissolved sample and fluxed for several hours to break down fluoride compounds that may still remain in the solution, then dried down. The sample was then dissolved with 1.5 mL of 2N HCl, dried down, dissolved in ~ 0.5 mL of 1N HBr, dried gently, re-dissolved in ~ 0.5 mL of 1N HBr, fluxed gently, centrifuged, and the solution was used for ion-exchange column chromatography.

Pb was first separated following a Pb column protocol outlined in Table1 using 250µl AG-1 x-8 200-400 mesh anion resin. A solution containing Hf, and the majority of the sample matrix, was eluted with HBr, followed by Pb collection with HCl. The following was done to the Pb eluent for MC-ICP-MS analysis:

1. Dry down the 6N HCl containing separated Pb
2. Dissolve precipitate in 0.1 mL of 15N HNO_3,
3. Dry again
4. Dissolve precipitate with 3% HNO_3, ready for MC-ICP-MS analysis.

Hf was then separated and purified in a two-step ion column chromatography method. The first column utilized 2 mL of AG 50W x-8 100-200 mesh cation resin, and the second column used a 200μl TODGA 50-100 μm resin. After collection from the first Hf column, the following was done to prepare the solution containing Hf for the second column:

1. Dry the 0.5N HCl + 0.15N HF fraction containing Hf
2. Dissolve precipitate in 0.375 mL of 15N HNO_3
3. Dry the solution
4. Dissolve precipitate in 0.85 mL 3.5N HNO_3 + 0.06N H_3BO_3, flux for ~10 min

Upon completing the protocol on the second Hf column using TODGA resin, these final steps were taken to prepare the sample for isotope analysis:

1. Dry the 2N HNO_3 + 0.35N HF fraction
2. Dissolve precipitate in 0.1 mL HNO_3
3. Dry the solution
4. Dissolve precipitate in 1mL of 3% HNO_3 + 0.035N HF

Pb and Hf were analyzed on a Thermo Scientific Neptune Multicollector-Inductively Coupled Plasma-Mass Spectrometer (MC-ICP-MS) to obtain $^{206}Pb/^{204}Pb$, $^{207}Pb/^{204}Pb$, $^{208}Pb/^{204}Pb$, and $^{176}Hf/^{177}Hf$ data for each sample. All Pb isotope ratios were corrected for interference from ^{204}Hg based on a $^{202}Hg/^{204}Hg$ ratio of 4.350370, while $^{176}Hf/^{177}Hf$ ratios were corrected for interference from ^{176}Lu based on a $^{175}Lu/^{176}Lu$ ratio of 37.61 (Galer, 1998; Vervoort and Blichert-Toft, 1999). Mass bias correction was also done within the instrument on the Hf ratios on the basis of $^{179}Hf/^{177}Hf = 0.7325$. Mass bias correction on Pb could not be conducted due to a lack of stable Pb isotopes. Following all of the corrections within the Neptune software, offline normalization on the samples to known standard values is conducted to further reduce error. Measured Hf ratios are normalized to the daily average of repeated measurements of the JMC-475 Hf standard and Pb ratios are normalized using a standard-sample-sample-standard bracketing method with the NBS-981 Pb standard. Standard values used for normalization are provided below (Galer, 1998; Vervoort and Blichert-Toft, 1999).

Hf Standard JMC 475 Value: $^{176}Hf/^{177}Hf = 0.282160$

Pb Standard NBS 981 Values: $^{206}Pb/^{204}Pb = 36.7219$

$^{207}Pb/^{204}Pb = 15.4963$

$^{208}Pb/^{204}Pb = 16.9405$

USGS powder standards AGV-2 and BHVO-2 were prepared following the same sample preparation protocol, and were analyzed with each elemental separation batch to ensure the validity and accuracy of the experimental process. Multiple solutions of the same standards were prepared and measured to analyze repeatability of the sample preparation protocol; individual solutions were also measured on multiple days to assess instrument variability.

Table 1.
Pb and Hf column separation procedure

Column 1: Pb Separation 0.25 mL AG 1-X8 Resin			Column 2: Hf Separation 2 mL AG50W-X8 100-200 Resin			Column 3: Hf Separation 0.20 mL 200µl TODGA 50-100 µm Resin		
Clean	4 CV	6N HCl	Clean	10 CV	6N HCl	Clean	10 CV	10.5N HNO_3
Rinse Reservoir		H_2O	Condition	6 CV	0.5N HCl	Clean	30 CV	2N HNO_3 + 0.35N HF
Clean	4 CV	H_2O	Load	0.5 CV	0.5N HCl	Clean	15 CV	0.05N HCl
Condition	4 CV	1N HBr	Collect Hf	1 CV	0.5N HCl + 0.15N HF	Condition	10 CV	3.5N HNO_3
Load & collect Hf	2 CV	1N HBr	Collect Hf	1 CV	0.5N HCl + 0.15N HF	Load	4.25 CV	3.5N HNO_3 + 0.06N H_3BO_3
Wash & Collect Hf	2 CV	1N HBr	Collect Hf	1.5 CV	0.5N HCl + 0.15N HF	Wash	17.5 CV	3.5N HNO_3
Wash & Collect Hf	4 CV	2N HCl				Collect Hf	10 CV	2N HNO_3 + 0.35N HF
Wash & Collect Pb	4 CV	6N HCl				Collect Hf	10 CV	2N HNO_3 + 0.35N HF
						Collect Hf	10 CV	2N HNO_3 + 0.35N HF
						Wash	15 CV	2N HNO_3 + 0.35N HF
						Wash	25 CV	0.5N HCl
						Wash	10 CV	0.05N HCl

Results

Table 2 contains the complete ^{206}Pb/^{204}Pb, ^{207}Pb/^{204}Pb, ^{208}Pb/^{204}Pb, and ^{176}Hf/^{177}Hf dataset. Pb and Hf ratios, the first Hf data from the Oregon Cascades, are consistent with existing Cascade arc data: ^{206}Pb/^{204}Pb = 18.821–19.022, ^{207}Pb/^{204}Pb = 15.576–15.617, ^{208}Pb/^{204}Pb = 38.391–38.424, and ^{176}Hf/^{177}Hf = 0.283032–0.283094 (ε_{Hf} = 9.19–11.38). εHf was calculated using the equation $\frac{(^{176}Hf/^{177}Hf)_{sample}-(^{176}Hf/^{177}Hf)_{CHUR}}{(^{176}Hf/^{177}Hf)_{CHUR}} * 10000$ using CHUR value of $^{176}Hf/^{177}Hf =$ 0.282772, and εNd was calculated using the equation $\frac{(^{143}Nd/^{144}Nd)_{sample}-(^{143}Nd/^{144}Nd)_{CHUR}}{(^{143}Nd/^{144}Nd)_{CHUR}} * 10000,$ using CHUR value of $^{143}Nd/^{144}Nd$=0.512638. (Blichert-Toft et al., 1997; DePaolo, 1988). Figure 4 presents data for all samples plotted using ^{144}Nd/^{143}Nd and ^{87}Sr/^{86}Sr isotope data that were normalized to values for NBS-987 (^{144}Nd/^{143}Nd = 0.710248) and La Jolla (^{87}Sr/^{86}Sr = 0.511858) respectively from Mitchell (2013). Data for USGS standards that were analyzed along with the lava samples are plotted in Figure 5. The andesite standard data, AGV-2, indicate minimal variability in isotope values throughout all of the data, and do not deviate from the literature value provided by Weis et al. (2006). The basalt standard BHVO-2, however, varies significantly between different powder batches, but shows that the same solution run multiple times shows relatively small variations. Such variation indicates that the standard itself may be heterogeneous, due to the error bar of BHVO-2 and the undisputable uniformity of the AGV-2 isotope values (Figure 5). The standard analyses validate our isotopic analysis methods within a very small margin of error.

The focus here is placed on the primitive samples, as they are the most representative of the parent magma that is created prior to differentiation as the magma undergoes extrusion. Other than the primitive samples clustering together (^{144}Nd/^{143}Nd = 0.521919 – 0.512975, ^{87}Sr/^{86}Sr = 0.703317 – 0.703541, ^{176Hf}/^{177}Hf = 0.283063 – 0.283085, ^{206}Pb/^{204}Pb = 18.901 – 18.951, ^{207}Pb/^{204}Pb = 15.586 – 15.602), there are no significant trends that can be identified with the Three Sisters isotope data.

However, a visibly noticeable trend in the Newberry data can be seen, reinforcing previous assumptions that more evolved samples are edging closer to an upper crustal felsic composition (Mitchell and Asmerom, 2011).

Table 2.

Pb-Hf isotope data for central Oregon Lavas.

Sample ID	^{206}Pb/^{204}Pb	^{207}Pb/^{204}Pb	^{208}Pb/^{204}Pb	^{206}Pb/^{208}Pb	^{206}Pb/^{207}Pb	^{176}Hf/^{177}Hf	εHf
Standards							
AGV-2	18.870	15.619	38.549	0.4897	1.2084	0.282973	7.12
BHVO-2	18.654	15.545	38.238	0.4880	1.2002	0.283104	11.73
Nash Crater							
08-LL-01	18.920 ± 4	15.596 ± 4	38.547 ± 11	0.4909 ± 1	1.2133 ± 2	0.283082 ± 3	10.97 ± 11
07-LN-01	18.894 ± 2	15.589 ± 2	38.527 ± 9	0.4905 ± 1	1.2121 ± 1	0.283037 ± 2	9.40 ± 7
08-NCSW-01	18.887 ± 5	15.589 ± 4	38.520 ± 10	0.4904 ± 0	1.2117 ± 0	0.283069 ± 2	10.53 ± 7
Sand Mountain							
08-SM-01	18.845 ± 4	15.583 ± 5	38.457 ± 17	0.4901 ± 1	1.2094 ± 1	0.283073 ± 2	10.64 ± 7
08-SMCL-01	18.807 ± 3	15.563 ± 2	38.390 ± 6	0.4900 ± 0	1.2086 ± 0	0.283066 ± 2	10.43 ± 1
07-NC-01	18.825 ± 3	15.575 ± 2	38.428 ± 7	0.4900 ± 0	1.2087 ± 1	0.283068 ± 3	10.50 ± 10
Belknap							
08-WBB-01	18.901 ± 2	15.586 ± 3	38.497 ± 10	0.4911 ± 1	1.2129 ± 1	0.283067 ± 3	10.46 ± 11
07-LB-01	18.881 ± 3	15.560 ± 2	38.443 ± 8	0.4912 ± 0	1.2135 ± 1	0.283050 ± 3	9.84 ± 10
07-BCB-02	18.888 ± 2	15.589 ± 2	38.516 ± 8	0.4905 ± 0	1.2118 ± 1	0.283039 ± 2	9.46 ± 9
Yapoah							
07-FCA-01	18.914 ± 2	15.597 ± 2	38.570 ± 1	0.4905 ± 1	1.2128 ± 1	0.283097 ± 3	11.52 ± 11
07-YC-02	18.857 ± 2	15.584 ± 2	38.486 ± 4	0.4901 ± 0	1.2101 ± 1	0.283056 ± 4	10.07 ± 13
07-CC-01	18.851 ± 1	15.581 ± 2	38.485 ± 6	0.4900 ± 0	1.2100 ± 1	0.283062 ± 3	10.26 ± 10
Newberry							
08-SPBF-01	18.960 ± 2	15.603 ± 3	38.583 ± 8	0.4911 ± 1	1.2154 ± 2	0.283076 ± 4	10.78 ± 13
08-FRF-01	18.954 ± 1	15.597 ± 2	38.566 ± 5	0.4910 ± 0	1.2154 ± 1	0.283063 ± 3	10.32 ± 10
08-LCFF-01	18.976 ± 2	15.601 ± 2	38.590 ± 6	0.4919 ± 0	1.2166 ± 1	0.283061 ± 3	10.23 ± 9
08-MBF-02	19.031 ± 6	15.624 ± 6	38.685 ± 15	0.4921 ± 1	1.2183 ± 1	0.283075 ± 3	10.71 ± 10
08-LBF-01	18.992 ± 2	15.607 ± 3	38.620 ± 10	0.4919 ± 1	1.2171 ± 1	0.283060 ± 2	10.20 ± 8
08-SF-01	19.001 ± 2	15.608 ± 4	38.623 ± 9	0.4921 ± 1	1.2176 ± 1	0.283063 ± 2	10.31 ± 7
Pre-Mazama							
08-WIC-01	18.943 ± 4	15.591 ± 3	38.533 ± 7	0.4918 ± 1	1.2153 ± 1	0.283071 ± 3	10.60 ± 11
08-CYC-01	18.928 ± 2	15.601 ± 3	38.594 ± 9	0.4906 ± 1	1.2134 ± 1	0.283062 ± 3	10.27 ± 10
08-EC-01	18.959 ± 2	15.603 ± 3	38.605 ± 11	0.4912 ± 1	1.2152 ± 1	0.283031 ± 4	9.19 ± 13

Table 3.

Sr-Nd isotope data for central Oregon lavas.

Sample ID	^{87}Sr/^{86}Sr	^{143}Nd/^{144}Nd	ε_{Nd}
Nash Crater			
08-LL-01	**0.703489**	**0.512951**	**6.1**
07-LN-01	0.703406	0.512915	5.4
08-NCSW-01	0.703368	0.512917	5.44
Sand Mountain			
08-SM-01	0.703214	0.512966	6.4
08-SMCL-01	0.703146	0.512961	6.3
07-NC-01	0.703205	0.512955	6.18
Belknap			
08-WBB-01	**0.703317**	**0.51297**	**6.48**
07-LB-01	0.703412	0.512908	5.27
07-BCB-02	0.703431	0.512909	5.29
Yapoah			
07-FCA-01	*0.703415*	*0.512955*	*6.18*
07-YC-02	0.703384	0.512912	5.34
07-CC-01	0.703537	0.512904	5.19
Newberry			
08-SPBF-01	***0.703452***	***0.512949***	***6.07***
08-FRF-01	0.703487	0.512925	5.59
08-LCFF-01	0.703527	0.512917	5.44
08-SF-01	0.70351	0.512923	5.56
08-LBF-01	0.703532	0.512914	5.38
08-MBF-02	0.703448	0.512938	5.84
Pre-Mazama			
08-WIC-01	**0.703392**	**0.512975**	**6.57**
08-CYC-01	**0.703541**	**0.512919**	**5.48**
08-EC-01	0.703893	0.51285	4.13
08-LC-01	0.703469	0.512927	5.64

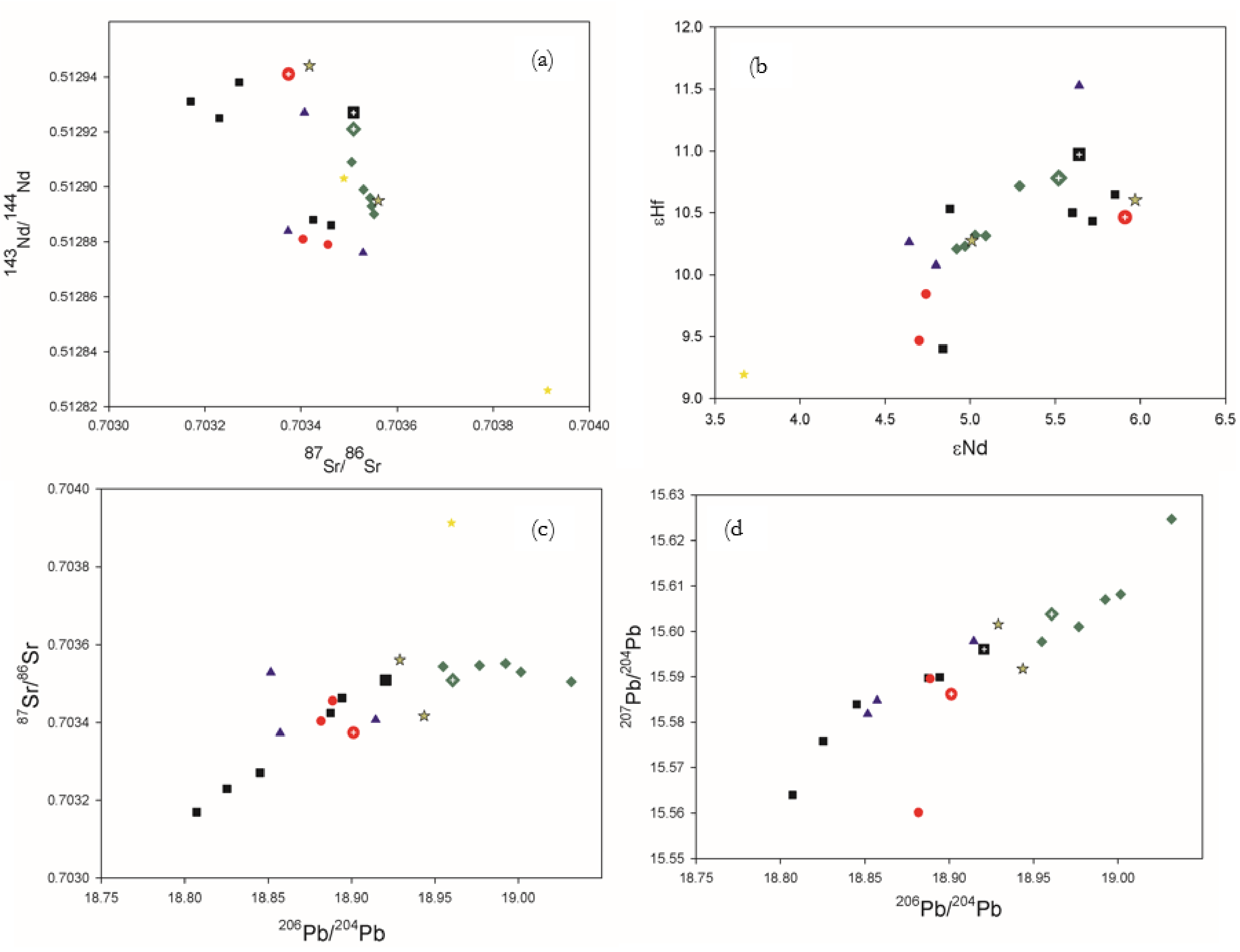

Figure 4: Isotope data from samples collected from the central Oregon Cascades (Figure 2). Symbols as Figure 2. Most primitive samples denoted with crosshairs, or outlined edges in black. a) ^{143}Nd/^{144}Nd vs. ^{87}Sr/^{86}Sr, b) ^{207}Pb/^{204}Pb vs. ^{206}Pb/^{204}Pb, c) εHf vs. εNd, d) ^{87}Sr/^{86}Sr vs. ^{206}Pb/^{204}Pb.

Table 4. Experimental standards

	$^{206}Pb/^{204}Pb$	$^{207}Pb/^{204}Pb$	$^{208}Pb/^{204}Pb$	$^{206}Pb/^{208}Pb$	$^{206}Pb/^{207}Pb$	$^{176}Hf/^{177}Hf$
Weis et al., 2006/2007						
AGV-2	18.868 ± 6	15.617 ± 7	38.544 ± 14			0.282984 ± 9
BHVO-2	18.647 ± 24	15.533 ± 9	38.236 ± 18			0.283105 ± 11
AGV-2a (1).	18.868 ± 5	15.619 ± 3	38.548 ± 10	0.4896 ± 0	1.2083 ± 1	0.282971 ± 3
AGV-2a(2).	18.871 ± 2	15.621 ± 2	38.553 ± 7	0.4896 ± 0	1.2083 ± 1	0.282972 ± 3
AGV-2b (1).	18.872 ± 2	15.619 ± 3	38.552 ± 9	0.4896 ± 1	1.2085 ± 1	0.282975 ± 3
AGV-2b (2).	18.867 ± 2	15.616 ± 3	38.541 ± 9	0.4897 ± 1	1.2084 ± 1	
AGV-2c (1).	18.871 ± 1	15.618 ± 1	38.549 ± 6	0.4896 ± 0	1.2084 ± 0	0.282973 ± 3
Average	**18.870**	**15.619**	**38.549**	**0.490**	**1.208**	**0.283**
SD	**0.004**	**0.004**	**0.009**	**0.0001**	**0.0002**	**0.0000**
BHVO Standards						
BHVO-2a (1).	18.535 ± 1	15.516 ± 4	38.123 ± 14	0.4864 ± 0	1.1951 ± 1	0.283101 ± 3
BHVO-2a (2).	18.543 ± 3	15.515 ± 2	38.123 ± 6	0.4864 ± 0	1.1952 ± 0	0.283101 ± 3
BHVO-2a (3).	18.549 ± 2	15.528 ± 3	38.157 ± 8	0.4862 ± 1	1.1948 ± 1	
BHVO-2b (1).	18.763 ± 3	15.559 ± 3	38.313 ± 9	0.4897 ± 1	1.2059 ± 1	0.283096 ± 3
BHVO-2b (2).	18.766 ± 3	15.569 ± 2	38.345 ± 9	0.4895 ± 0	1.2055 ± 1	0.283101 ± 3
BHVO-2b (3).	18.767 ± 2	15.569 ± 2	38.342 ± 8	0.4896 ± 1	1.2056 ± 1	
BHVO-2c (1).	18.694 ± 4	15.529 ± 5	38.226 ± 12	0.4893 ± 3	1.2043 ± 6	0.283121 ± 3
BHVO-2c (2).	18.682 ± 3	15.546 ± 2	38.261 ± 9	0.4884 ± 1	1.2019 ± 1	
BHVO-2c (3).	18.683 ± 3	15.548 ± 4	38.266 ± 13	0.4884 ± 1	1.2018 ± 1	
BHVO-2d (1).	18.555 ± 2	15.569 ± 2	38.223 ± 7	0.4856 ± 0	1.1919 ± 1	0.283099 ± 3
Average	**18.654**	**15.545**	**38.239**	**0.488**	**1.200**	**0.283**
SD	**0.198**	**0.043**	**0.167**	**0.003**	**0.011**	**0.000003**

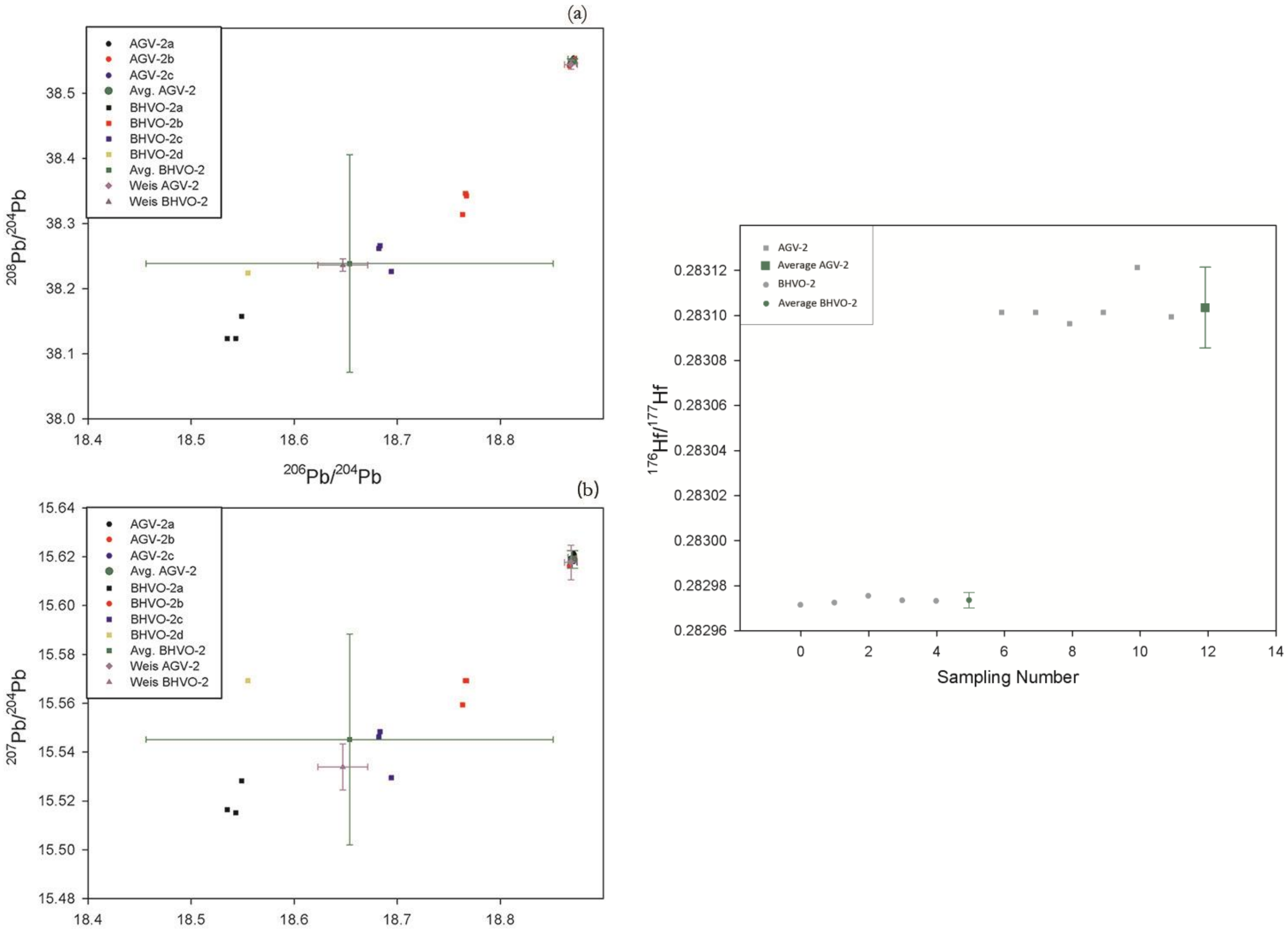

Figure 5: Pb and Hf data for USGS standards AGV-2 and BHVO-2 measured during the course of the study. Multiple different powders of each standard were analyzed, and each powder was analyzed on multiple days. Letters indicate the separate powders analyzed. a) $^{207}Pb/^{204}Pb$ vs. $^{206}Pb/^{204}Pb$ for all standards run, error bars placed on the average values and the literature value provided by Weis et al. (2006). b) $^{208}Pb/^{204}Pb$ vs. $^{206}Pb/^{204}Pb$ for all standards analyzed, and error bars placed on the same samples as (a). c) $^{177}Hf/^{176}Hf$ plot on all of the standard samples, error bars shown on average values. Tabulated values of these standard values located in Table 3.

Discussion

Comparison with existing Cascades and relevant regional data

Major and trace element data have been provided and discussed by Mitchell (2013). Comparison of the Three Sisters data with other mafic flows suggests a relatively similar composition to other isotope data from different parts of the Cascades. Potential end member reservoirs that contribute to the composition of arc basalts, the mantle wedge and the subducting sediments, are plotted in Figure 6. The subducting oceanic crust also contributes to the lava composition, and its contribution is discussed in the section titled *Altered Ocean Crust* in the Discussion. These plots include data from regional MORBs that are used as a proxy for the mantle end member, and sediments from the Deep Sea Drilling Program (DSDP) and Ocean Drilling Program(ODP) that are used as a proxy for the sediment end member in the models (Carpentier et al., 2014; Prytulak et al., 2006). Isotopic values for a homogeneous mantle wedge end member are determined by taking the average of all of the MORB isotope data, and end member values for the sediments were determined by obtaining an average for each of the distinct sediment cores from the JdF plate.

Modeling framework

In order to analyze the role of fluids in the magma genesis of the central Oregon Cascades, contributions of the mantle wedge and sediment reservoirs are constrained using radiogenic isotopes. Analyzing $^{87}Sr/^{86}Sr$, $^{143}Nd/^{144}Nd$, $^{206}Pb/^{204}Pb$, $^{207}Pb/^{204}Pb$, $^{208}Pb/^{204}Pb$, and $^{176}Hf/^{177}Hf$ data obtained from Mitchell (2013) and this project, the sediment contribution from each of the drilling sites can be investigated through a variety of mixing models. The simplest model created is the bulk addition model, where mixing of the mantle and bulk sediment end members is simulated through a

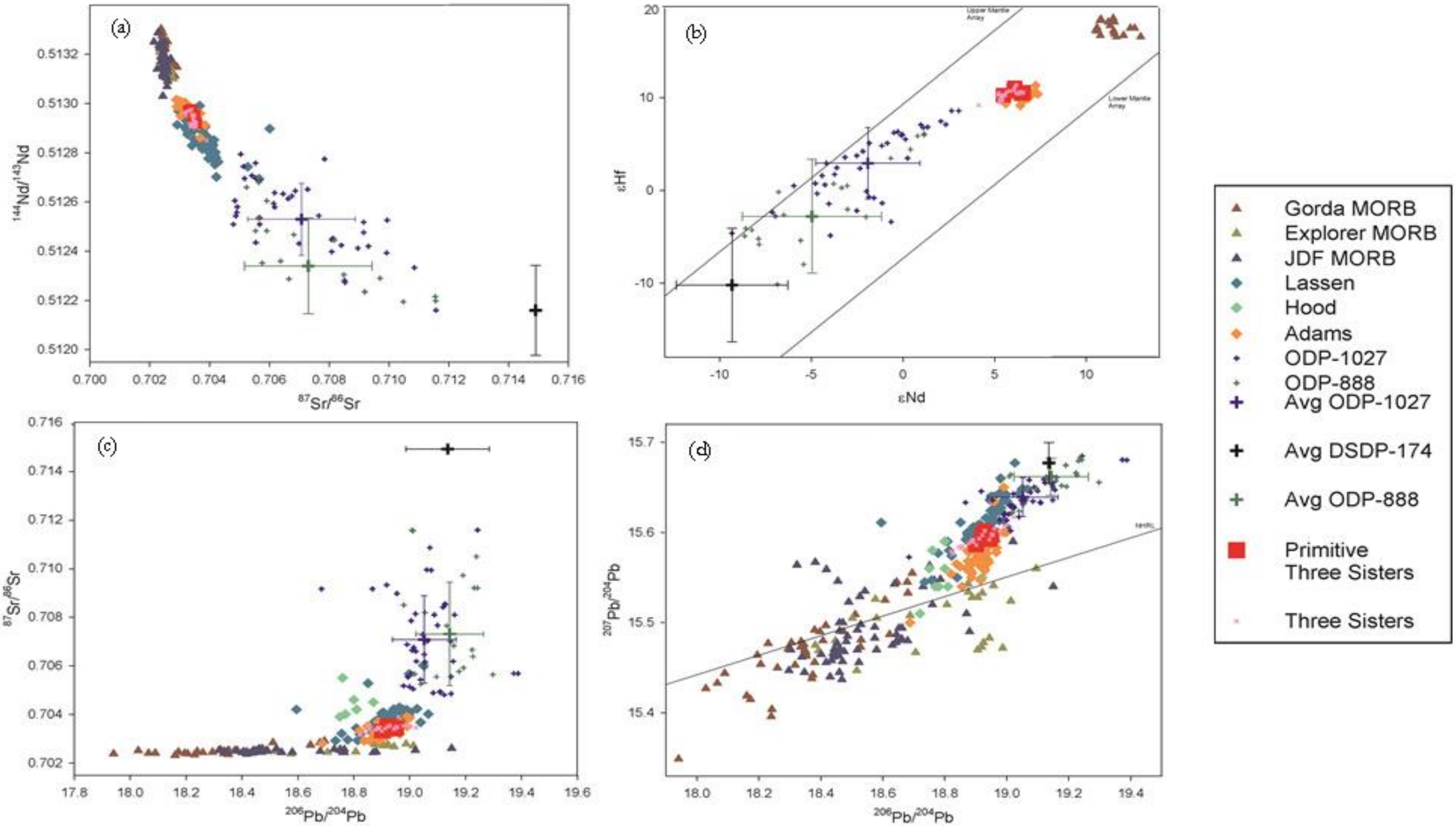

Figure 6: Radiogenic isotope data for the central Oregon lavas, along with relevant published data from the Cascades region. a) ^{143}Nd/^{144}Nd vs. ^{87}Sr/^{86}Sr, b) ^{207}Pb/^{204}Pb vs. ^{206}Pb/^{204}Pb, c) εHf vs. εNd, d) ^{87}Sr/^{86}Sr vs. ^{206}Pb/^{204}Pb. Sediment data ODP sites 888 and 1027, and DSDP site 174 on the Juan de Fuca plate (Figure 1). 1σ error bars on the sediment data, illustrating relative compatibility with the measured Oregon lava data. MORB data compiled from the Explorer, Juan de Fuca, and Gorda plates. Lava isotope data from other volcanoes and vents in the Cascades. The sediment and MORB data used to generate end member data for modeling acting as the sediment and mantle proxies, respectively. Isotope data from other volcanoes have similar values with the central Oregon lavas, suggesting a basic consistency in isotope data throughout the Cascades. Sediment data obtained from Carpentier (2014) and Prytulak (2006); MORB and Cascades volcanic data obtained from numerous sources downloaded within the EarthChem database.

two component mixing equation:

$$R_m^i = \frac{R_A^i C_A^i + R_B^i\, C_B^i(1-f).}{C_A^i F + C_B^i(1-f).} \qquad \boxed{\text{Equation 1}}$$

where R^i_M is the isotope ratio of element *i* in the mixture, R^i_A is the isotope ratio of element *i* in component A (i.e. mantle), R^i_B is the isotope ratio of element *i* in component B (i.e. sediment), C^i_A is the concentration of element *i* in component A, C^i_B is the concentration of element *i* in component B, and *f* is the proportion of component A in the mixture. Figure 7 demonstrates the variance between model curves simulating different mechanisms of slab contribution and thermal conditions despite having the same end member isotopic ratios. The trajectories of the curves vary due to the calculated elemental concentration values for each distinct mechanism and thermal condition constrained in the model. The concentration terms in Equation 1 determine the curvature of the hyperbolic mixing line and fit with the central Oregon Cascades lava data, which is the main factor in the following modeling analyses.

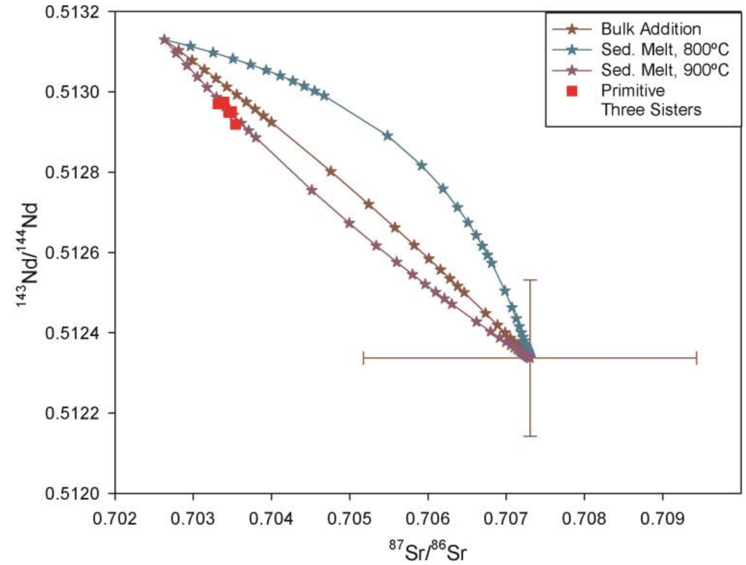

Figure 7. An example of a slab component modeling plot for the central Oregon lavas. The sediment end member value is from the ODP site 888 (Carpentier et al, 2014), and a value for a homogeneous mantle end member is used. Modeling curves denote different slab contribution mechanisms or thermal conditions for the same end member values, where the curves are a function of the elemental contribution.

More complex models simulate partial melting of the subducting slab at high temperatures and two or three component mixing between this sediment melt, a fluid phase, and the mantle end member. Fluid and melt compositions of the model are calculated using a batch, modal melting equation (Shaw, 1970) and experimentally derived bulk partition coefficients, or D values (Table 5). The batch melting equation is:

$$C^l/C^o = \frac{1}{D_o + F(1 - D_o).} \qquad \boxed{\text{Equation 2}}$$

where C^l/C^O is the concentration of the element in the melt divided by the concentration of the element in the original solid, D_o is the bulk partition coefficient, and F is the extent of melting.

Bulk addition and one-step melt modeling

Though bulk addition of the subducting sediment is likely not a realistic process of slab contribution in arc systems, a recent proposal that arc magmas may be generated through melting of a mélange-diapir has justified modeling a simplified version of this process (Marschall and Schumacher, 2012). Plots of bulk addition (Figure 8) of the three sediment end members to the mantle wedge indicate that such a process does not produce best-fit curves to the data. Modeling curves with a 50% modal melt of sediments at 800ºC are also included in the same plots (Figure 8), and do not show significant variation from the bulk addition simulations. The Hf-Nd fit of the 50% melt model shows notable improvement in the curve trajectory, as shown by difference in proximity to the central Oregon Cascades data compared to the bulk modeling. However, the Nd-Sr plot is compromised, indicating an equal amount of decline in the fit of the model curve. Despite the better fit of the Hf-Nd curves, the worsened fit of the Sr-Nd plot indicates that this model does not sufficiently replicate the thermal conditions of sediment melting. The significant shifts in the curves can be attributed to the sediment melt D_o value of Nd at 800ºC (D_o = 2.27), indicating that Nd is compatible at this temperature and remains in the melt residue (Skora and Blundy, 2010).

Thus, not all plots in Figure 8 provide equally good fits, and the sediment proportion varies throughout the different plots. A majority of the plots, with the exception of the Hf-Nd and Sr-Nd plots of sediment melt at 800ºC, indicate that sediments contribute approximately 0.2 – 1.0% of the mantle wedge composition. When taking the 1σ error bars from the sediment data into account, along with the improved fit of the Hf-Nd plot, the possibility of these processes dominating the sediment contribution is feasible. Given the complexity of the subsurface arc system of the Cascades, and the lack of a consistent sediment source providing the closest fit, either more complex or different processes contributing to these isotope values is likely.

Table 5.
D_o Values

	Sr	Pb	Nd	Hf	Sm
Sediments					
650ºC[a]	0.53	0.64	3.26	5.3*	
800ºC[b]	0.0667	0.0667	2.2727	0.7692	
900ºC[b]	0.0323	0.0300	0.6667	0.3333	
AOC					
900ºC[c]	0.0474	0.0588	0.6623	0.5882	
Accessory Minerals					
Clinopyroxene[d]			0.36	0.67	0.55
Garnet[e]			0.52	0.25	0.24
Rutile[f]			0.0003	0.0009	40
Zircon[g]			0.0220	0.2420	64600
Monazite[h]			76400	75300	1

[a] Plank (2014)
[b] Skora and Blundy (2010)
[c] Klemme (2005)
[d] Blundy et al. (1998)
[e] Chauvel and Blichert-Toft (2001)
[f] Tatsumi and Hanyu (2003)
[g] Rubatto and Hermann (2003)
[h] Bea and Montery (1999)

Table 6.

End member values

	$^{87}Sr/^{86}Sr$	[Sr]	$^{144}Nd/^{143}Nd$	[Nd]	$^{176}Hf/^{177}Hf$	[Hf]	$^{206}Pb/^{204}Pb$	[Pb]	$^{207}Pb/^{204}Pb$	[Pb]
DMM[a]	0.70263	7.664	0.513130	0.581	0.283500	0.157	18.275	0.018	15.486	0.018
ODP-888[b]	0.70764	314	0.512384	20.25	0.282693	3.925	19.157	12.275	15.659	12.275
ODP-1027[b]	0.70978	314	0.512540	20.25	0.282855	3.925	19.064	12.275	15.637	12.275
DSDP-174[c]	0.71490	323	0.512124	27.968	0.282483	4.825	19.162	14.5	15.680	14.500

[a] Workman et al. (2005), Su and Langmuir (2003)

[b] Carpentier et al. (2014)

[c] Prytulak et al. (2006).

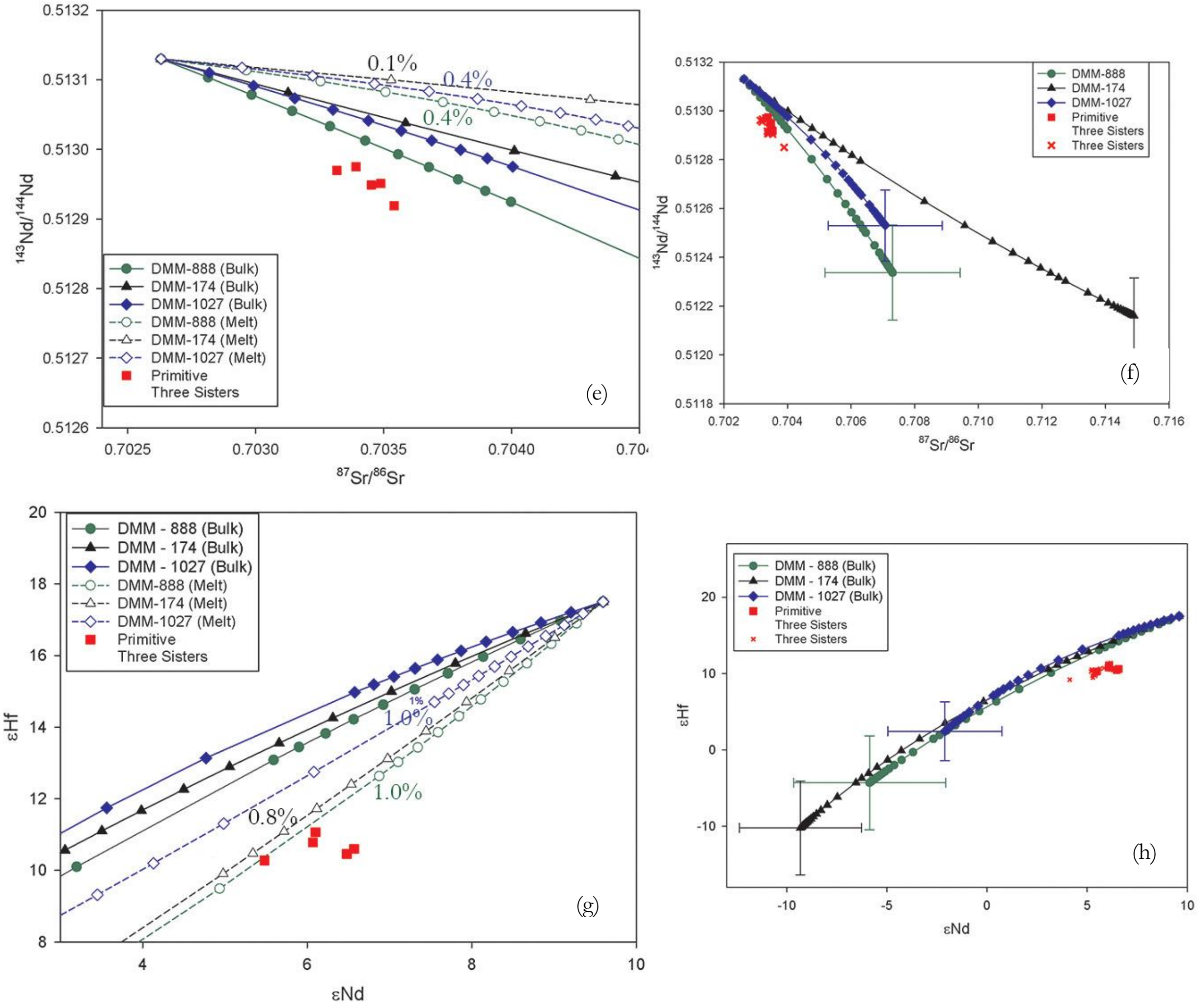

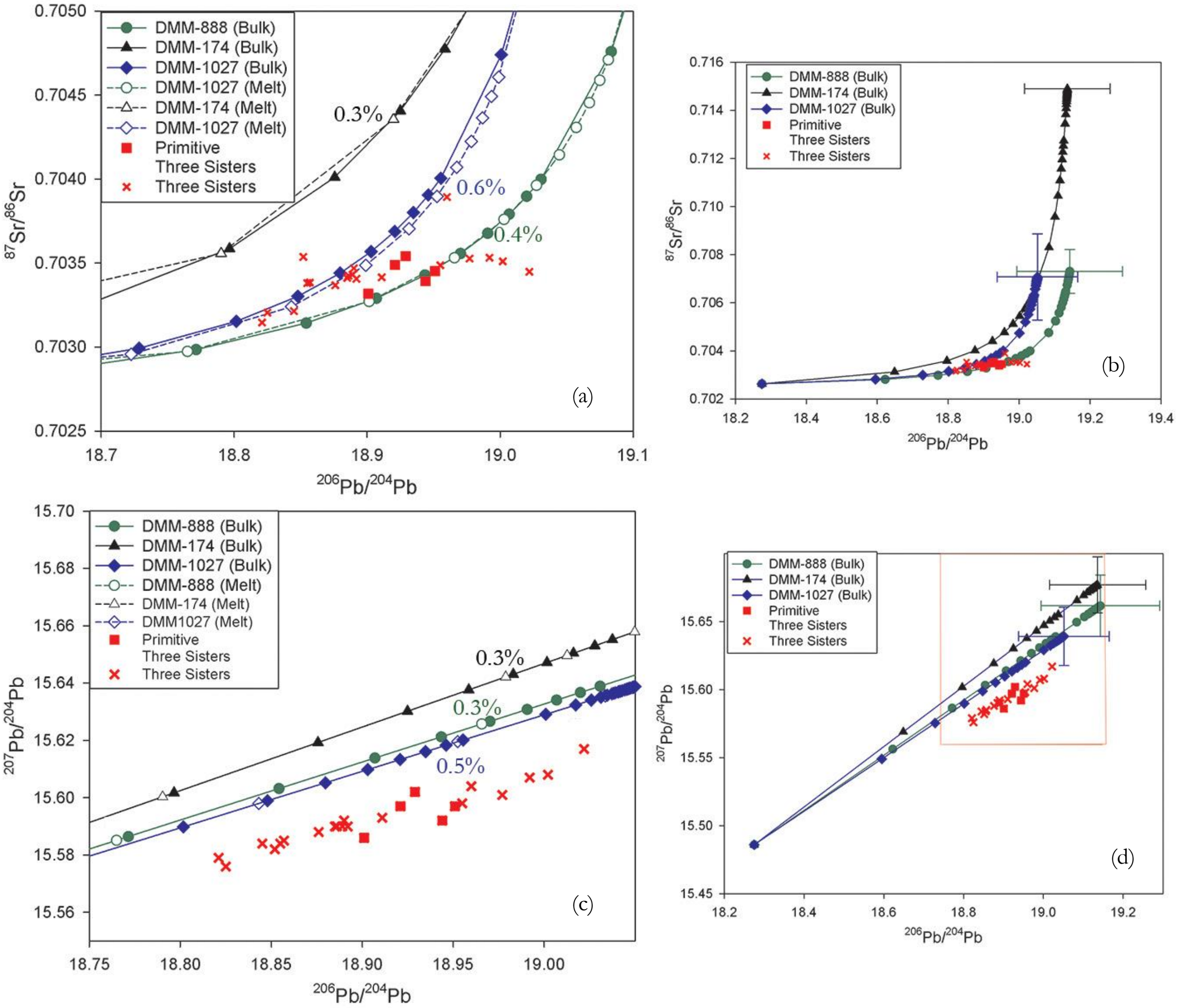

Figure 8: Slab component modeling plot for central Oregon lavas. Solid lines and points indicate modeling plots using a bulk addition model, while dotted curves with hollow points simulate a 50% melt of the sediments at 800ºC mixing into the mantle wedge. a) Zoomed in plot of (b), both ^{143}Nd/^{144}Nd vs. ^{87}Sr/^{86}Sr comparisons. c) Zoomed in plot of (d), both ^{207}Pb/^{204}Pb vs. ^{206}Pb/^{204}Pb comparisons. e) Zoomed in plot of (f), both εHf vs. εNd comparisons. g) Zoomed in plot of (h), both ^{87}Sr/^{86}Sr vs. ^{206}Pb/^{204}Pb comparisons. Values in the graphs indicate the contribution of the sediment into the wedge, which consistently ranges from 0.2 – 1.0%. Special emphasis is placed on the primitive central Oregon lava data, which best represents the mantle wedge. MORB and sediment end member data, and partition coefficients used for the 50% melt can be found in Table 5. Composition of the mantle source and sediment sources can be found in Table 6.

Two-step melting

Due to the limitations of bulk addition and one-step melt models, a two-step melt process has been simulated in an attempt to improve the fit of the curves (Figure 9). In this proposed system, a 10% melt of the subducting sediment at 800ºC is removed from the system, and the remaining slab residue undergoes 50% melting at 900ºC. The batch melt equation (Eqn. 2) used in the one-melt modeling is used again in both steps of the melting process; the only differences are the extent of melting in the first step, and the partition coefficient value used in the second step to melt the slab at higher temperatures (Table 6).

The ^{143}Nd/^{144}Nd vs. ^{87}Sr/^{86}Sr plot of the two-step melting shows a better fit with the central Oregon isotope data, along with the ^{87}Sr/^{86}Sr vs. ^{206}Pb/^{204}Pb plot that already had curves intersect the primitive lava data in the simpler models. Modeling of ^{207}Pb/^{204}Pb vs. ^{206}Pb/^{204}Pb neither improves nor worsens the fit, suggesting that Pb is unaffected by the change in the partition coefficients related to higher thermal conditions. The εHf vs. εNd plot is the only curve that worsens, influenced by the incompatibility of Nd ($D_o = 0.67$). However, the fit of Hf-Nd does not worsen considerably, while the Sr-Nd curves match with the data remarkably. The sediment contribution range of 0.2 – 1.0% is confirmed with the modeling plots of the two-step melt. In the ^{207}Pb/^{204}Pb vs. ^{206}Pb/^{204}Pb plot, the concentration ratios of the two components do not vary, explaining the mixing curve's straight trajectory in all models. On the other hand, it is difficult to ascertain Hf's static modeling behavior, which may be due to Hf's relatively inconsequential change in D_o values between 800ºC and 900ºC.

This two-step model shows better fits with the central Oregon data, but this model is still unable to produce satisfactory fits on all isotope parameters studied. Dehydration of the slab prior to melting, as opposed to two separate episodes of melting, is likely a more realistic process of magma genesis because the subducting slab experiences hotter temperatures at lower pressures (Spandler and Pirard, 2013). Taking dehydration into account and modeling dehydration before melting could potentially produce curves with better fits to the measured central Oregon data. The improved fit of the two-step melt modeling suggests that a more complex fluid addition process probably takes place beneath the Cascade arc. The plots also affirm that the melting conditions of the slab can occur at higher temperatures (> 800ºC), which is consistent with the uncommon thermal conditions of the Cascades.

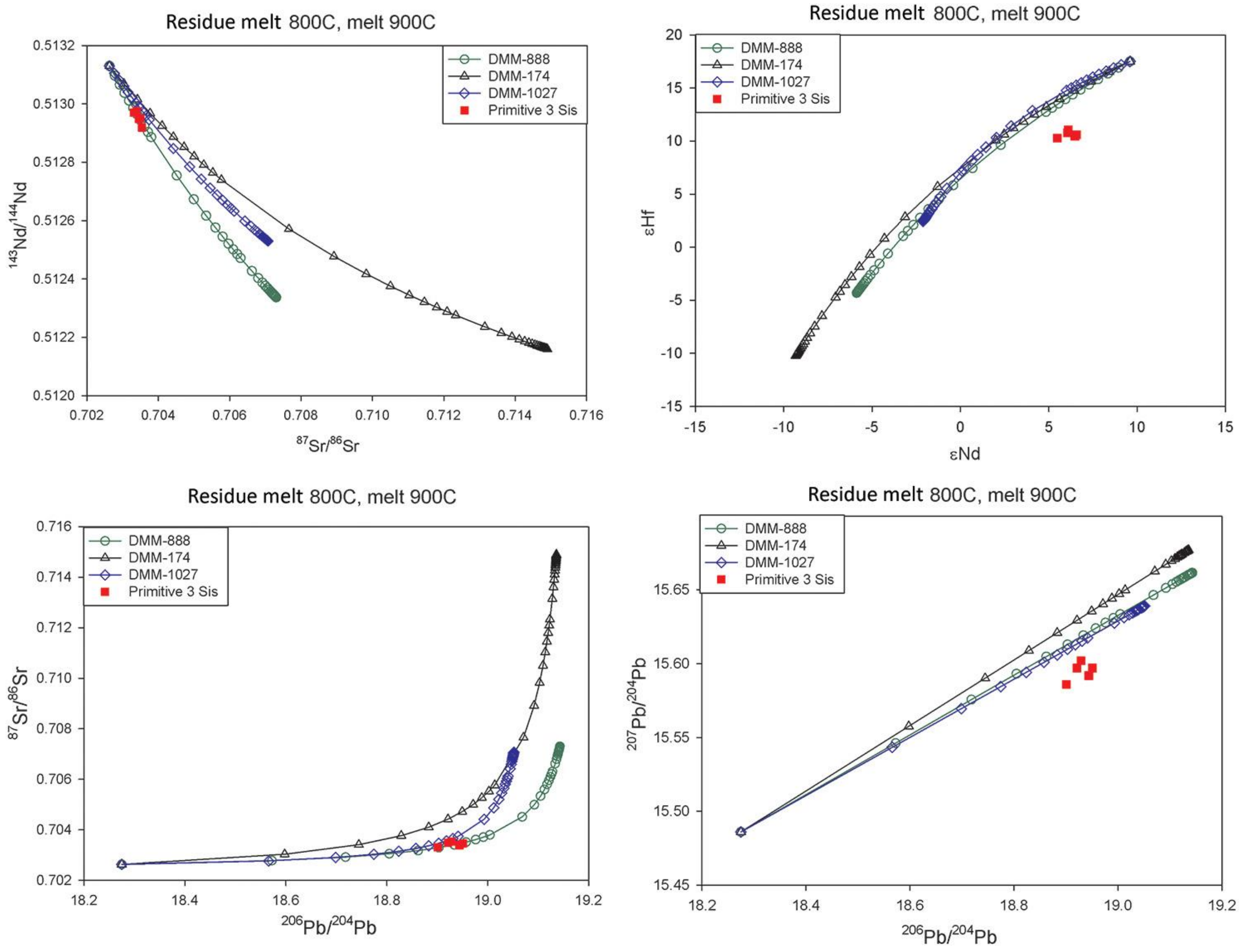

Figure 9: Slab component modeling plot for the central Oregon Cascades simulating a two-step melt process. A 10% melt of subducting sediments at 800ºC is removed from the system, followed by a second 50% melt event at 900ºC. a) ^{143}Nd/^{144}Nd vs. ^{87}Sr/^{86}Sr, b) ^{207}Pb/^{204}Pb vs. ^{206}Pb/^{204}Pb, c) εHf vs. εNd, d) ^{87}Sr/^{86}Sr vs. ^{206}Pb/^{204}Pb. Composition of the mantle source and the sediment sources can be found in Table 6. Partition coefficient values of the sediment melt at specific temperatures can be found in Table 5.

Varying melt temperatures

It is likely that sediments may begin to dehydrate at lower temperatures than 800ºC. Although modeling a dehydration event at a lower temperature could potentially improve the fits of the model curves with the central Oregon data, there is currently no dataset of sediment partition coefficients at these conditions that provides values for all four elements of interest. Johnson and Plank (1999) provide partition coefficient values at subsolidus conditions at ~3GPa for all of the elements of interest except for Hf. Hence, a partition coefficient was inferred relative to experimentally determined and published values for other geochemically similar elements (Table 5).

The best fit model involves 50% dehydration of the subducting sediments at 650ºC, followed by a 50% melt of the remaining slab residue at 900ºC that subsequently mixes with the mantle wedge (Figure 10). When comparing the two sets of two-step models created, it is evident that simulating lower temperature dehydration produces an overall better fit with the central Oregon Cascades data. However, the Sr-Pb isotope mixing curve moves away from the 888 and 1027 curves towards the 174 sediment curve, but these trajectory movements are minimal. In addition, the Pb-Pb plot curves do not move for the reasons explained above. In addition, since the partition coefficient of Hf was not experimentally determined, the validity of the most improved model (Hf-Nd) is debatable. The relatively good fit of the models with the central Oregon data indicates that a two-step dehydration-melting process over a several hundred degree temperature range is a reasonable approximation for the evolution of the Juan de Fuca plate beneath the Cascades. The sediment contribution still ranges from roughly 0.2 - 1.0% again; 174 sediments have lower sediment contributions than other sediments (0.3 - 0.6 %), while 888 and 1027 sediments maintain the original range (0.2 – 1.0%). These contribution ranges reaffirm the proposed contribution of the subducting sediments to the magma composition.

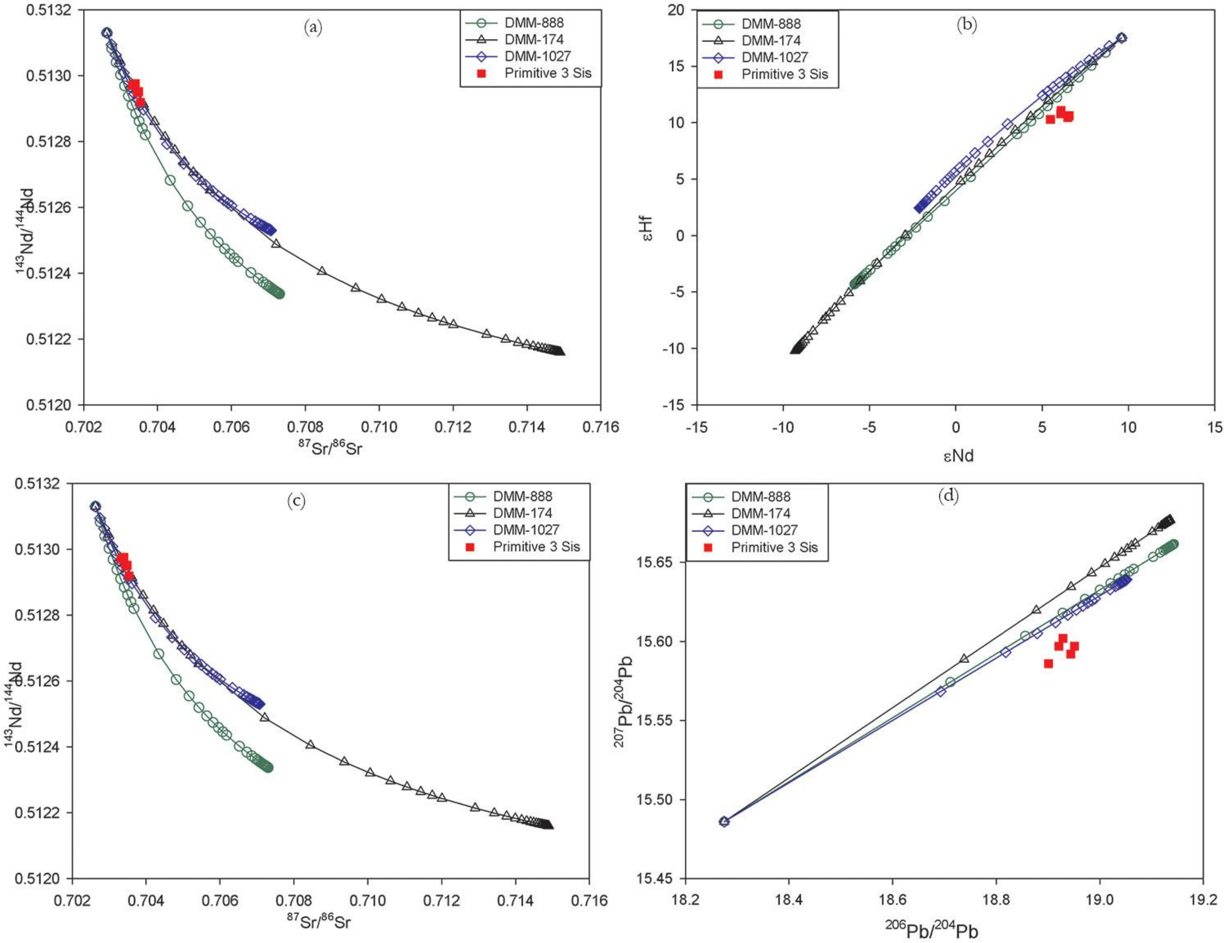

Figure 10: Slab component modeling plot of central Oregon Cascades simulating a two-step dehydration-melting process. 50% of the fluid in the subducting sediments is removeded at 650ºC, then the remaining residue undergoes 50% melting at 900C a) ^{143}Nd/^{144}Nd vs. ^{87}Sr/^{86}Sr, b) ^{207}Pb/^{204}Pb vs. ^{206}Pb/^{204}Pb, c) εHf vs. εNd, d) ^{87}Sr/^{86}Sr vs. ^{206}Pb/^{204}Pb. The partition coefficient of Hf was not reported for dehydration experiments at 650ºC, so the Hf value was inferred to be 5.3 for the provided thermal conditions. Composition of the mantle source and the sediment sources can be found in Table 6. Partition coefficient values of the sediment melt at specific temperatures can be found in Table 5.

Altered ocean crust

The altered oceanic crust can contribute to the magma composition through dehydration or melting of that crust (Mullen and McCallum, 2014) Since there was no available isotopic composition and elemental concentration data for the AOC end member, these values had to be estimated.

The isotope values correlating to the sediment contribution value from the melt curve (10% and 30% sediment contribution) was used as sediment end member, while the AOC end member was derived by mixing the calculated AOC value with the bulk DMM value. Elemental concentrations were derived using a two-component mixing equation ($C_i = C_i^{mantle} * f^{mantle} + C_i^{AOC} * f^{AOC}$, C = concentration of the end member, f = proportion of the component in the mixture). Two sets of concentrations were independently calculated, one for the 10% AOC model curve and another for the 30% AOC model curve.

Taking dehydration of the ocean crust into account prior to the melting processes at higher temperatures such as the two-step modeling has produced models that reproduce the data; however, models show very high contributions from the slab and suggest that these models are unrealistic. Attempts at modeling the AOC contribution through dehydration have not produced conclusive results. Of the isotopic parameters studied, Nd, Pb, and Hf isotope data may lead to misleading or incorrect models. Hf can be found in subducting oceanic crust and Nd is abundant in the oceanic crust; thus, the crust's contribution could be negligible because the subducting crust is very similar to the MORB mantle wedge (Kessel et al., 2005). This similarity can also hinder Pb analyses; a component derived from AOC can be masked in Pb-Pb plots due to the AOC's isotopic similarity to that of the mantle wedge, although the extent of these discrepancies remains uncertain (Mullen and McCallum, 2014).

Though AOC contribution is very likely, modeling this component has not been successful from the central Oregon Cascades data. Further analyses and modeling efforts can help elucidate this issue and potentially create model curves that provide better fits than the current ones presented in this project.

Accessory mineral modeling

Decoupling between trace element migration and fluid loss during devolatilization has been observed during subduction-based metamorphism (Miller et al., 2007; Spandler et al., 2003). This implies that the mobilization of trace elements including Sr, Nd, Hf, and Pb is low during slab dehydration, and the presence and stabilities of certain accessory minerals present in the metamorphosed AOC and sediments exert a strong control over trace element abundances (EL Korh et al., 2009). Accessory mineral stability in the subducting slab is influenced by many factors, including temperature (Frost, 2006). Therefore, assessing the presence of accessory minerals in the subducting slab of the central Oregon Cascades could potentially determine the temperature at which sediment melt is occurring.

Along with negative Hf anomalies in the Cascadia sediment, it is expected to see negative Hf concentration anomalies in the central Oregon Cascades (Carpentier et al., 2014). Hf concentration anomalies are quantified by Hf/Hf*, where Hf* = $\frac{Nd_{CI}+Sm_{CI}}{(2)}$. The CI chondrite values used in this calculation can be found in the Figure 11 captions. Hf anomaly quantifies Hf's relative compatibility in the melt compared to the compatibilities of Sm and Nd, and important accessory minerals have large partition coefficients for Sm, Nd, or Hf. Consequently, modeling should be sensitive to the presence of very small amounts of these minerals in the residual phase during sediment melting.

Following Tollstrup and Gill's (2005) sediment non-modal melt modeling for the presence of accessory minerals including zircon, rutile, and monazite, a similar model has been constructed for the central Oregon lavas (Figure 11). Bulk partition coefficients have been specifically calculated based on the presence or absence of the accessory minerals, as shown in Table 5. Values from the ODP and DSDP drilling are still used as the sediment end members, while the homogeneous mantle is still assumed as the mantle end member from the combination of MORB data. Hf anomalies are compared with Hf isotopes by modeling the composition of the sediment melt by adding rutile, zircon, and monazite to the residue in succession.

The initial residue is eclogitic, containing clinopyroxene and garnet, and modeling curves created from these conditions have a less negative Hf anomaly than the central Oregon lavas. Previous results indicate that rutile, as well as zircon, may be responsible for the negative Hf anomalies found in arc lavas (Wade et al., 2005). Consequently, adding 3.5% rutile into the system, where the partition coefficient of Hf in rutile is much higher than those of clinopyroxene and garnet (Table 5), lowers the curve trajectory to make the curves pass through the central Oregon lava values. Next, 0.003% zircon, known to be present in the residue of sediment melting experiments, was added to the residual model system now composed of clinopyroxene, garnet, and rutile. Hf is extremely compatible in zircon, resulting in poorer fits to the curves. Since the partition coefficients of Nd and Sm are very high in monazite, while Hf has a low partition coefficient, monazite was then introduced to the proposed model. Introducing 0.003% of monazite to complement the compatibility of Hf in zircon did reduce the Hf anomaly of the model curves, but the anomaly was reduced too much to match with the central Oregon lavas. Because such a small amount of zircon and monazite have been added to the modeling system, reducing the amounts of these accessory minerals in the residue would improve the fits of models with zircon and monazite, but reducing an already negligible amount of zircon and monazite is likely unrealistic in an arc system.

Tollstrup and Gill (2005) suggest that samples from the cooler Mariana arc can be explained by sediment melts that are saturated with trace accessory minerals including zircon, rutile, and monazite. However, modeling such accessory phases with samples from the central Oregon Cascades is not consistent with these findings. Through the sediment and residual phase modeling created in Figure 11, it can be inferred that rutile is present in the sediment melt residue in the Juan de Fuca plate beneath the central Oregon Cascades, while zircon and monazite are not. The combination of isotope and Hf anomaly analyses suggests that slab temperatures during sediment melting are hot enough for zircon and monazite to no longer be stable in the residue, but for rutile to persist. Experimental data suggest that this implies subducted sediment melting temperatures of greater than 800 ºC, although other factors, such as the extent of melting, are also important (Hermann and Rubatto, 2009).

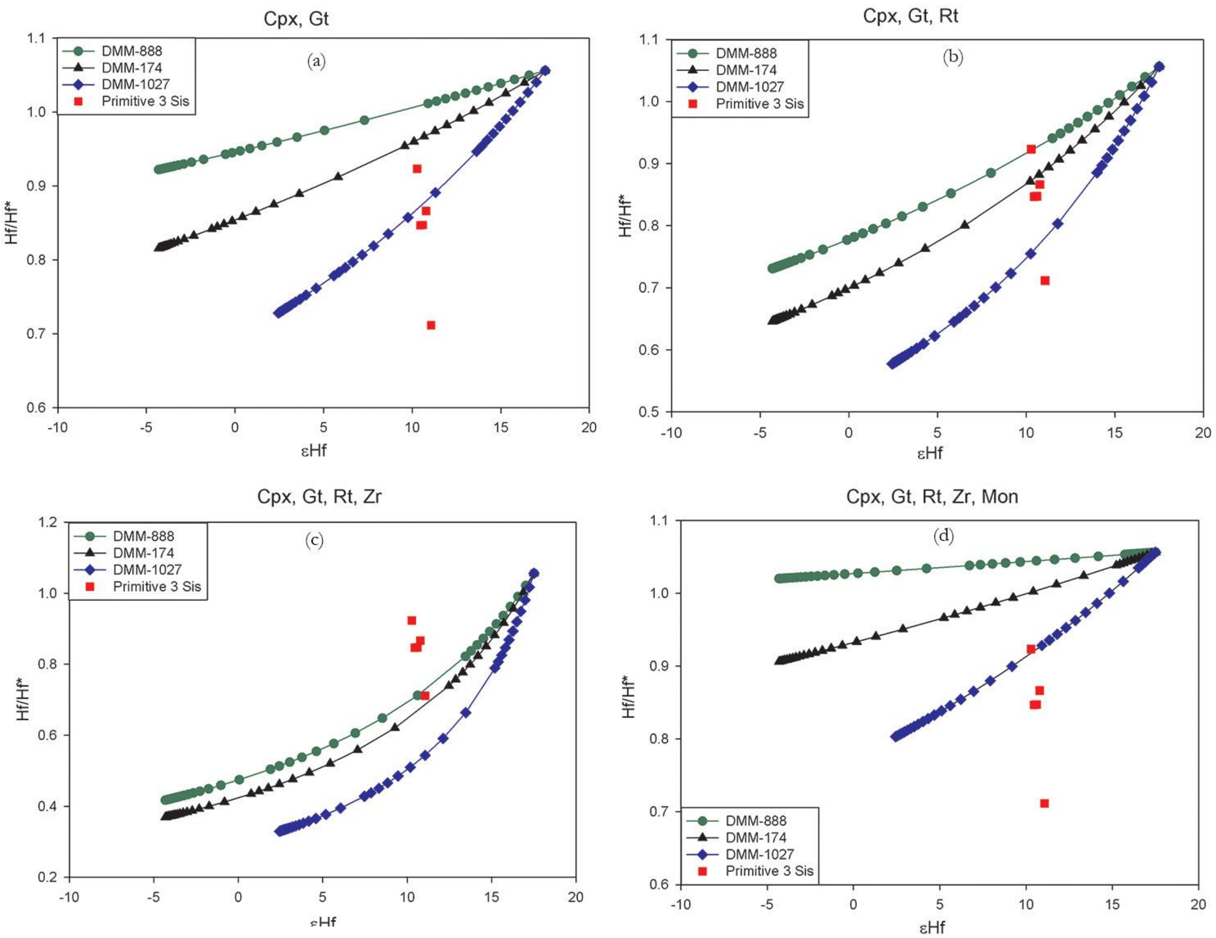

Figure 11: Hf/Hf* vs. εHf accessory mineral component modeling plot for central Oregon Cascades lavas. a) Plot of a melt residue model with clinopyroxene and garnet. b) Plot of a melt residue model with clinopyroxene, garnet, and rutile. c) Plot of a melt residue model with clinopyroxene, garnet, rutile, and zircon. d) Plot of a melt residue model with clinopyroxene, garnet, rutile, and monazite. Hf/Hf* = $[(Hf/Hf_N) / [(Sm/Sm_N) + (Nd/Nd_N) / 2]$, and illustrates relative depletion of Hf compared to Nd and Sm (Hf/Hf* < 0) CI values: Hf = 0.103, Sm = 0.148, Nd = 0.457 (McDonough and Sun 1995). Composition of the mantle source and the sediment sources can be found in Table 6. Partition coefficient values of the sediment melt at specific temperatures can be found in Table 5.

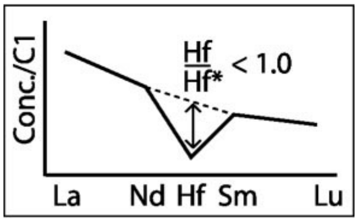

Conclusion

This project contributes Hf and Pb isotope data ($^{176}Hf/^{177}Hf$, $^{206}Pb/^{204}Pb$, $^{207}Pb/^{204}Pb$, and $^{208}Pb/^{204}Pb$) for mafic lava flows from the Three Sisters volcanoes and Newberry Volcanic Field areas in the central Oregon Cascades. Radiogenic isotope data gathered in this project have been combined with prior analyses that included major, trace, and isotope data conducted by Mitchell (2013).

Isotope data modeling provides insights into the magma genesis process in the central Oregon Cascades. It is inferred that sediments in the subducting slab contribute to the magma composition. Modeling results suggest that a multi-step dehydration and/or melting process is a more plausible mechanism for introducing slab components into the mantle asthenosphere than a single-step process. The data are consistent with approximately 0.2 – 1.0% of the subducted sediments being incorporated into the mantle source.

In addition, accessory mineral modeling provides a qualitative insight into the melting conditions of the subducting slab. While minerals such as zircon and monazite are commonly assumed to be present as residual phases during slab dehydration or melting, the unusual thermal conditions of the central Oregon Cascades do not allow these two minerals to remain stable in the sediment melt residue. However, the presence of residual rutile is supported by the data. These observations place upper and lower limits on the temperature at which sediment melting is occurring beneath the arc, and therefore on the overall thermal structure of the Cascadia subduction zone.

References

Bacon, C.R., Gunn, S.H., Lanphere, M.A., Wooden, J.L., 1994. Multiple Isotopic Components in Quaternary Volcanic Rocks of the Cascade Arc near Crater Lake, Oregon. J. Petrol. 35, 1521–1556. doi:10.1093/petrology/35.6.1521

Bas, M.J.L., Maitre, R.W.L., Streckeisen, A., Zanettin, B., IUGS Subcommission on the Systematics of Igneous Rocks, 1986. A Chemical Classification of Volcanic Rocks Based on the Total Alkali-Silica Diagram. J. Petrol. 27, 745–750. doi:10.1093/petrology/27.3.745

Blichert-Toft, J., Chauvel, C., Albarède, F., 1997. Separation of Hf and Lu for high-precision isotope analysis of rock samples by magnetic sector-multiple collector ICP-MS. Contrib. Mineral. Petrol. 127, 248–260. doi:10.1007/s004100050278

Borg, L.E., Brandon, A.D., Clynne, M.A., Walker, R.J., 2000. Re–Os isotopic systematics of primitive lavas from the Lassen region of the Cascade arc, California. Earth Planet. Sci. Lett. 177, 301–317. doi:10.1016/S0012-821X(00)00051-0

Carpentier, M., Weis, D., Chauvel, C., 2014. Fractionation of Sr and Hf isotopes by mineral sorting in Cascadia Basin terrigenous sediments. Chem. Geol. 382, 67–82. doi:10.1016/j.chemgeo.2014.05.028

Churikova, T., 2001. Sources and Fluids in the Mantle Wedge below Kamchatka, Evidence from Across-arc Geochemical Variation. J. Petrol. 42, 1567–1593. doi:10.1093/petrology/42.8.1567

Conrey, R.M., Sherrod, D.R., Hooper, P.R., Swanson, D.A., 1997. Diverse primitive magmas in the Cascade arc, Northern Oregon and Southern Washington. Can. Mineral. 35, 367–396.

Conrey, R.M., Taylor, E.M., Donnelly-Nolan, J.M., Sherrod, D.R., 2002. North central Oregon Cascades: Exploring petrologic and tectonic intimacy in a propagating intra-arc rift, in

Moore, G.W., ed. Field Guide Geol. Process. Cascadia Or. Dep. Geol. Miner. Ind. Spec. Pap. 47–90.

DePaolo, D.J., 1988. Neodymium isotope geochemistry: an introduction, Minerals and rocks. Springer-Verlag, Berlin ; New York.

Eagar, K.C., Fouch, M.J., James, D.E., Carlson, R.W., 2011. Crustal structure beneath the High Lava Plains of eastern Oregon and surrounding regions from receiver function analysis. J. Geophys. Res. 116. doi:10.1029/2010JB007795

EL Korh, A., Schmidt, S.T., Ulianov, A., Potel, S., 2009. Trace Element Partitioning in HP-LT Metamorphic Assemblages during Subduction-related Metamorphism, Ile de Groix, France: a Detailed LA-ICPMS Study. J. Petrol. 50, 1107–1148. doi:10.1093/petrology/egp034

Frost, D.J., 2006. The Stability of Hydrous Mantle Phases. Rev. Mineral. Geochem. 62, 243–271. doi:10.2138/rmg.2006.62.11

Galer, S.J.G., 1998. Practical Application of Lead Triple Spiking for Correction of Instrumental Mass Discrimination. Mineral. Mag. 62A, 491–492. doi:10.1180/minmag.1998.62A.1.260

Govers, R., Meijer, P.T., 2001. On the dynamics of the Juan de Fuca plate. Earth Planet. Sci. Lett. 189, 115–131. doi:10.1016/S0012-821X(01)00360-0

Green, N.L., Sinha, A.K., 2005. Consequences of varied slab age and thermal structure on enrichment processes in the sub-arc mantle of the northern Cascadia subduction system. J. Volcanol. Geotherm. Res. 140, 107–132. doi:10.1016/j.jvolgeores.2004.07.017

Grove, T., Parman, S., Bowring, S., Price, R., Baker, M., 2002. The role of an H2O-rich fluid component in the generation of primitive basaltic andesites and andesites from the Mt. Shasta region, N California. Contrib. Mineral. Petrol. 142, 375–396. doi:10.1007/s004100100299

Guffanti, M., Weaver, C.S., 1988. Distribution of Late Cenozoic volcanic vents in the Cascade range: Volcanic arc segmentation and regional tectonic considerations. J. Geophys. Res. 93, 6513. doi:10.1029/JB093iB06p06513

Hermann, J., Rubatto, D., 2009. Accessory phase control on the trace element signature of sediment melts in subduction zones. Chem. Geol. 265, 512–526. doi:10.1016/j.chemgeo.2009.05.018

Hildreth, W.H., 2007. Quaternary magmatism in the Cascades; geologic perspectives. US Geol. Surv. Prof. Pap. 1–136.

Hochstaedter, A., Gill, J., Peters, R., Broughton, P., Holden, P., Taylor, B., 2001. Across-arc geochemical trends in the Izu-Bonin arc: Contributions from the subducting slab: ACROSS-ARC GEOCHEMICAL TRENDS. Geochem. Geophys. Geosystems 2, n/a–n/a. doi:10.1029/2000GC000105

Jicha, B.R., Hart, G.L., Johnson, C.M., Hildreth, W., Beard, B.L., Shirey, S.B., Valley, J.W., 2009. Isotopic and trace element constraints on the petrogenesis of lavas from the Mount Adams volcanic field, Washington. Contrib. Mineral. Petrol. 157, 189–207. doi:10.1007/s00410-008-0329-6

Kessel, R., Schmidt, M.W., Ulmer, P., Pettke, T., 2005. Trace element signature of subduction-zone fluids, melts and supercritical liquids at 120–180 km depth. Nature 437, 724–727. doi:10.1038/nature03971

Leeman, W.P., Lewis, J.F., Evarts, R.C., Conrey, R.M., Streck, M.J., 2005. Petrologic constraints on the thermal structure of the Cascades arc. J. Volcanol. Geotherm. Res. 140, 67–105. doi:10.1016/j.jvolgeores.2004.07.016

Marschall, H.R., Schumacher, J.C., 2012. Arc magmas sourced from mélange diapirs in subduction zones. Nat. Geosci. 5, 862–867. doi:10.1038/ngeo1634

McBirney, A.R., White, C.M., 1982. The Cascade Province. In: Thorpe RS (ed) Andesites: orogenic andesites and related rocks. Wiley 115–135.

Miller, C., Zanetti, A., Thoni, M., Konzett, J., 2007. Eclogitisation of gabbroic rocks: Redistribution of trace elements and Zr in rutile thermometry in an Eo-Alpine subduction zone (Eastern Alps). Chem. Geol. 239, 96–123. doi:10.1016/j.chemgeo.2007.01.001

Mitchell, E.C., 2013. Uranium-series isotope constraints on magma generatin and differentation in the central Oregon Cascades. University of New Mexico, Department of Earth and Planetary Sciences.

Mitchell, E.C., Asmerom, Y., 2011. U-series isotope systematics of mafic magmas from central Oregon: Implications for fluid involvement and melting processes in the Cascade arc. Earth Planet. Sci. Lett. 312, 378–389. doi:10.1016/j.epsl.2011.09.060

Mullen, E.K., McCallum, I.S., 2014. Origin of Basalts in a Hot Subduction Setting: Petrological and Geochemical Insights from Mt. Baker, Northern Cascade Arc. J. Petrol. 55, 241–281. doi:10.1093/petrology/egt064

Mullen, E.K., Weis, D., 2013. Sr-Nd-Hf-Pb isotope and trace element evidence for the origin of alkalic basalts in the Garibaldi Belt, northern Cascade arc: Alkalic Basalts, Northern Cascade Arc. Geochem. Geophys. Geosystems 14, 3126–3155. doi:10.1002/ggge.20191

Pearce, J.A., Stern, R.J., 2006. Origin of back-arc basin magmas: Trace element and isotope perspectives, in: Christie, D.M., Fisher, C.R., Lee, S.-M., Givens, S. (Eds.), Geophysical Monograph Series. American Geophysical Union, Washington, D. C., pp. 63–86.

Prytulak, J., Vervoort, J.D., Plank, T., Yu, C., 2006. Astoria Fan sediments, DSDP site 174, Cascadia Basin: Hf–Nd–Pb constraints on provenance and outburst flooding. Chem. Geol. 233, 276–292. doi:10.1016/j.chemgeo.2006.03.009

Reiners, P.W., Hammond, P.E., McKenna, J.M., Duncan, R.A., 2000. Young basalts of the central Washington Cascades, flux melting of the mantle, and trace element signatures of primary arc magmas. Contrib. Mineral. Petrol. 138, 249–264. doi:10.1007/s004100050561

Rowe, M.C., Kent, A.J.R., Nielsen, R.L., 2009. Subduction Influence on Oxygen Fugacity and Trace and Volatile Elements in Basalts Across the Cascade Volcanic Arc. J. Petrol. 50, 61–91. doi:10.1093/petrology/egn072

Ruscitto, D.M., Wallace, P.J., Johnson, E.R., Kent, A.J.R., Bindeman, I.N., 2010. Volatile contents of mafic magmas from cinder cones in the Central Oregon High Cascades: Implications for magma formation and mantle conditions in a hot arc. Earth Planet. Sci. Lett. 298, 153–161. doi:10.1016/j.epsl.2010.07.037

Schmidt, M.E., Grunder, A.L., Rowe, M.C., 2008. Segmentation of the Cascade Arc as indicated by Sr and Nd isotopic variation among diverse primitive basalts. Earth Planet. Sci. Lett. 266, 166–181. doi:10.1016/j.epsl.2007.11.013

Skora, S., Blundy, J., 2010. High-pressure Hydrous Phase Relations of Radiolarian Clay and Implications for the Involvement of Subducted Sediment in Arc Magmatism. J. Petrol. 51, 2211–2243. doi:10.1093/petrology/egq054

Spandler, C., Hermann, J., Arculus, R., Mavrogenes, J., 2003. Redistribution of trace elements during prograde metamorphism from lawsonite blueschist to eclogite facies; implications for deep subduction-zone processes. Contrib. Mineral. Petrol. 146, 205–222. doi:10.1007/s00410-003-0495-5

Spandler, C., Pirard, C., 2013. Element recycling from subducting slabs to arc crust: A review. Lithos 170-171, 208–223. doi:10.1016/j.lithos.2013.02.016

Stolper, E., Newman, S., 1994. The role of water in the petrogenesis of Mariana trough magmas. Earth Planet. Sci. Lett. 121, 293–325. doi:10.1016/0012-821X(94)90074-4

Su, Y., Langmuir, C.H., 2003. Global MORB chemistry compilation at the segment scale (Department of Earth and Environmental Sciences). Columbia University.

Syracuse, E.M., van Keken, P.E., Abers, G.A., 2010. The global range of subduction zone thermal models. Phys. Earth Planet. Inter. 183, 73–90. doi:10.1016/j.pepi.2010.02.004

Tatsumi, Y., 1995. Subduction zone magmatism, Frontiers in earth sciences. Blackwell Science, Cambridge, Mass., USA.

Vervoort, J.D., Blichert-Toft, J., 1999. Evolution of the depleted mantle: Hf isotope evidence from juvenile rocks through time. Geochim. Cosmochim. Acta 63, 533–556. doi:10.1016/S0016-7037(98)00274-9

Wada, I., Wang, K., He, J., Hyndman, R.D., 2008. Weakening of the subduction interface and its effects on surface heat flow, slab dehydration, and mantle wedge serpentinization. J. Geophys. Res. 113. doi:10.1029/2007JB005190

Wade, J.A., Plank, T., Stern, R.J., Tollstrup, D.L., Gill, J.B., O'Leary, J.C., Eiler, J.M., Moore, R.B., Woodhead, J.D., Trusdell, F., Fischer, T.P., Hilton, D.R., 2005. The May 2003 eruption of Anatahan volcano, Mariana Islands: Geochemical evolution of a silicic island-arc volcano. J. Volcanol. Geotherm. Res. 146, 139–170. doi:10.1016/j.jvolgeores.2004.11.035

Workman, R.K., Hart, S.R., 2005. Major and trace element composition of the depleted MORB mantle (DMM). Earth Planet. Sci. Lett. 231, 53–72. doi:10.1016/j.epsl.2004.12.005

Xue, M., Allen, R.M., 2007. The fate of the Juan de Fuca plate: Implications for a Yellowstone plume head. Earth Planet. Sci. Lett. 264, 266–276. doi:10.1016/j.epsl.2007.09.047